Title

Fluorescence Excitation Emission Matrices of Human Tissue: A System for in vivo Measurement and Method of Data Analysis

Journal

Applied Spectroscopy, 53(3)

ISSN

0003-7028

Authors

Zuluaga, Andrés F
Utzinger, Urs
Durkin, Anthony
et al.

Publication Date

1999-03-01

DOI

10.1366/0003702991946695

Fluorescence Excitation Emission Matrices of Human Tissue: A System for *in Vivo* Measurement and Method of Data Analysis

ANDRÉS F. ZULUAGA, URS UTZINGER, ANTHONY DURKIN, HOLGER FUCHS, ANN GILLENWATER, RHONDA JACOB, BONNIE KEMP, JAMES FAN, and REBECCA RICHARDS-KORTUM *

Department of Electrical and Computer Engineering, The University of Texas at Austin, Austin, Texas 78712 (A.F.Z., U.U., H.F., R.R.-K.); Candela Corporation, Wayland, Massachusetts (A.D.); and Department of Head and Neck Surgery, The UT MD Anderson Cancer Center, Houston, Texas 77030 (A.G., R.J., B.K.)

We describe a system capable of measuring spatially resolved reflectance spectra from 380 to 950 nm and fluorescence excitation emission matrices from 330 to 500 nm excitation and 380 to 700 nm emission *in vivo*. System performance was compared to that of a standard scanning spectrofluorimeter. This "FastEEM" system was used to interrogate human normal and neoplastic oral cavity mucosa *in vivo*. Measurements were made through a fiber-optic probe and require 4 min total measurement time. We present a method based on autocorrelation vectors to identify excitation and emission wavelengths where the spectra of normal and pathologic tissues differ most. The FastEEM system provides a tool with which to study the relative diagnostic ability of changes in absorption, scattering, and fluorescence properties of tissue.

Index Headings: **Fluorescence; Reflectance; EEM; Tissue; Head and neck; Neoplasia.**

INTRODUCTION

A growing number of clinical studies have demonstrated that fluorescence spectroscopy can be used to distinguish normal and abnormal human tissues *in vivo* in the skin,[1] head and neck,[2,3] genito-urinary tract,[4,5] gastro-intestinal tract,[6,7] breast,[8] and brain.[9] References 10–13 provide recent reviews of this field. It is well known that fluorescence intensity and line shape are a function of both the excitation and emission wavelength in samples containing multiple chromophores, such as human tissue. A complete characterization of the fluorescence properties of an unknown sample requires measurement of a fluorescence excitation emission matrix, in which the fluorescence intensity is recorded as a function of both excitation and emission wavelength. The field of analytical chemistry has exploited the fluorescence properties of different compounds to identify and quantify them in mixtures. Holland et al.[14] described a computer-based system to measure fluorescence and absorbance simultaneously from quinine bisulfate. Warner and colleagues[15] built an instrument to collect a matrix of 241 fluorescence spectra at 241 different excitation wavelengths in 16.7 ms and used it to analyze the fluorescence properties of mixtures of hydrocarbons. Linear algebra methods were then applied to determine quantitative concentration and number of analyte data from these measurements.[16–19] These methods assume a linear system and are much more successful in nonscattering, optically dilute samples than they are in human tissue. In tissue, chromophores are embedded in a scattering and absorbing medium affecting both the excitation light reaching the chromophores and the emission light leaving the sample. The relationship between the fluorescence spectra of dilute and turbid samples has been explored[20] and found to be highly nonlinear. Studies have also been carried out investigating the performance of different linear algebra methods in the determination of concentrations and number of chromophores present in a homogeneous turbid sample.[21] However, it is not clear that they can be applied to inhomogeneous tissues.

Most clinical studies reported to date have measured fluorescence emission spectra at only a small number of excitation wavelengths (typically one to three) due to clinical requirements imposed on the size, speed, and sensitivity of instrumentation. The choice of excitation wavelength has been based on factors which vary from study to study, but include laser availability,[22] predictions of chromophores thought to be present in normal and abnormal tissues, and measurements of fluorescence excitation emission matrices (EEMs) of normal and abnormal tissues *in vitro*.[23,24] While *in vitro* measurements of tissue EEMs are feasible with the use of commercially available scanning fluorimeters, several studies have demonstrated that the optical properties of tissue change significantly when tissue is examined *in vitro* due in part to interruption of the blood supply,[25] oxidation,[26] and small size of biopsies.[27] Thus, *in vitro* studies to select excitation wavelengths are of limited value.

It is well known that the absorption and scattering properties of tissues *in vivo* affect both the intensity and line shape of measured fluorescence spectra.[28] The optical properties of tissue vary spatially, depending on its architecture, blood supply, and metabolic state; however, spatially resolved measurements of diffusely reflected light can be used to estimate tissue optical properties *in vivo*.[29–33] Several recent studies have suggested that differences in these optical properties, assessed by using diffuse reflectance spectroscopy, can be used to discriminate normal and abnormal human tissues *in vivo* in the urinary bladder[34] and the skin.[35] Furthermore, measuring both fluorescence and diffuse reflectance spectra may provide additional information of diagnostic value.[36,37]

A system capable of measuring spatially resolved reflectance spectra and fluorescence excitation emission matrices *in vivo* would remove the limitations of many

Received 16 July 1998; accepted 3 November 1998.
* Author to whom correspondence should be sent.

0003-7028/99/5303-0302$2.00/0

previous studies, potentially enabling prediction of those excitation wavelengths which provide greatest discrimination of normal and abnormal tissues, as well as a better understanding of the relative diagnostic ability of changes in absorption, scattering, and fluorescence properties of tissue. Two fiber-optic systems to record fluorescence EEMs and reflectance spectra at a single spatial location have been previously described in the literature.[38,39] Zuclich and colleagues[39] developed a fiber-optic system to record both diffusely reflected excitation light and fluorescence emission by using a single 14 bit multichannel detector. Sequential measurements were made, first with white light to collect the diffuse reflectance spectrum and then at a series of excitation wavelengths to collect both elastic backscattering and any induced fluorescence. Light was provided by a pulsed, filtered arc lamp from 300 to 600 nm in 10 nm increments, and following measurement, all spectra were assembled to yield the diffuse reflectance spectrum and a fluorescence EEM for a single spatial location. Collection of elastic backscattering and fluorescence EEMs from nonscattering tissues such as the human lens required 1–2 min. Typically, the elastic backscattering was at least 3–4 orders of magnitude stronger than the detected fluorescence, leaving a very limited dynamic range available to measure tissue fluorescence.

More recently, Zangaro et al.[38] described a system to record excitation emission matrices and diffuse reflectance from a single spatial location. A N_2 laser that pumps a series of 10 dye-containing cuvettes mounted on a rotating wheel provides sequential excitation at 11 different wavelengths from 337 to 500 nm; multichannel detection at each excitation wavelength yields 11 emission spectra that are then assembled to yield the excitation emission matrix. White light illumination is then used to produce a single diffuse reflectance spectrum. Collection of a tissue EEM and reflectance spectrum requires approximately 600 ms at a signal-to-noise ratio (SNR) of 50:1 for colon tissue.

In this paper we describe a system for *in vivo* measurement of fluorescence excitation emission matrices and spatially resolved diffuse reflectance spectra. An arc lamp coupled to a scanning spectrometer provides continuously tunable excitation light, which is coupled into a fiber-optic probe. Resulting tissue fluorescence is collected through the fiber probe and delivered to an imaging spectrograph and charge-coupled device (CCD) camera. Fluorescence emission spectra are collected sequentially at 18 excitation wavelengths ranging from 330 to 500 nm, which are then assembled into a fluorescence EEM. Subsequently, white light is coupled into the probe, and diffusely reflected light exiting the tissue at three spatial locations is detected from 380 to 950 nm by using the spectrograph and CCD. With this system, tissue EEMs and reflectance spectra with SNR in excess of 25:1 can be collected in approximately 4 min. We present EEMs and reflectance spectra of normal human oral cavity mucosa and a tumor of the oral cavity obtained *in vivo*. Finally, we describe a new method, based on excitation and emission autocorrelation vectors, to analyze fluorescence EEMs to determine excitation and emission wavelength regions where differences between normal and abnormal tissues are greatest. We illustrate the application of this method to the EEMs.

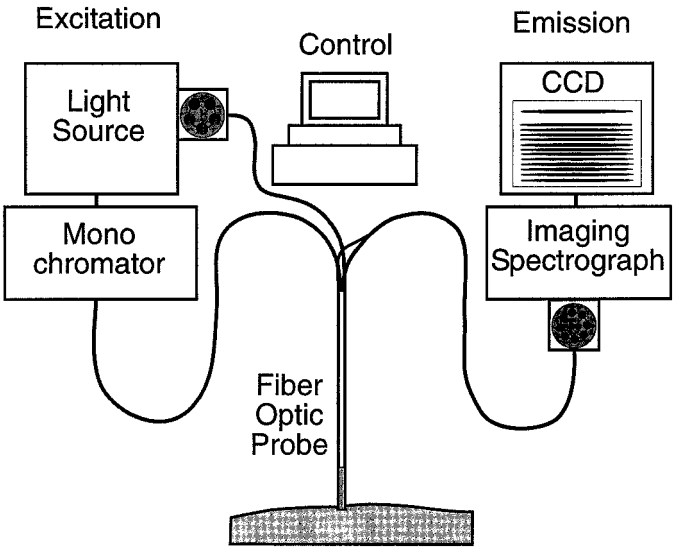

FIG. 1. System block diagram showing a variable excitation light source, a fiber-optic delivery and collection probe, and a spectral multichannel analyzer.

MATERIALS AND METHODS

Figure 1 illustrates a block diagram of the system (FastEEM system). The system consists of three main components: (1) an arc lamp, stepper motor-driven monochromator, and filter wheel, which provides monochromatic and broad band excitation; (2) a fiber-optic probe that directs excitation light to the tissue and collects remitted fluorescence from one location and diffusely reflected light from three locations; and (3) a filter wheel, imaging spectrograph, and CCD camera that detects the spectrally resolved reflectance and fluorescence signals. Excitation monochromator position, filter wheel position, spectrograph grating position, CCD operation, and data acquisition are controlled by a laptop personal computer mated to a docking station. The specifications of each sub-system are described below.

The probe, illustrated in Fig. 2, consists of a total of 46 optical fibers [200 μm diameter, numerical aperture (NA) = 0.2] arranged in two concentric bundles. The center bundle contains 25 fluorescence excitation fibers and 12 fluorescence collection fibers. The proximal ends of the fluorescence excitation fibers are arranged in two vertical lines at the exit slit of the excitation monochromator to maximize the coupling of the light into the sample. The proximal ends of the fluorescence collection fibers are arranged in a single vertical line at the entrance slit of the imaging spectrograph. At the distal end of the probe, the fibers that excite and collect fluorescence are arranged randomly in a central bundle and placed in contact with a short piece of a thick quartz fiber (2 mm diameter, 15 mm long, NA = 0.2). The distal tip of this fiber is placed in contact with the sample surface and ensures that the area from which fluorescence is collected is the same as that directly illuminated.

The nine fibers for illumination and collection of diffuse reflectance are arranged in a concentric ring around the thick quartz fluorescence measurement fiber. The distal ends of these fibers are flush with the tip of the central fiber and are placed in contact with the sample surface.

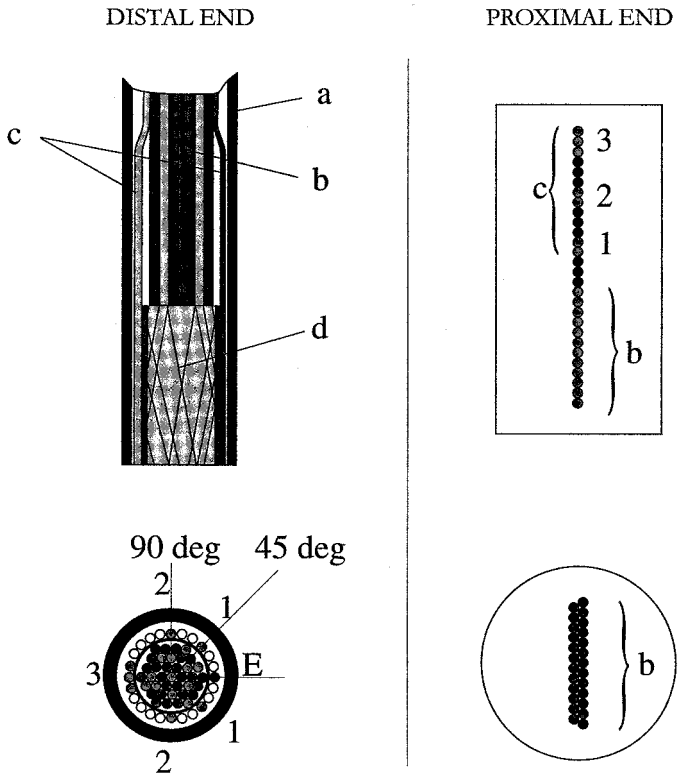

FIG. 2. (Left) Schematic diagram of the distal ends of the probe: (**a**) outer shaft, (**b**) fluorescence excitation and emission fibers, (**c**) reflectance collection and illumination fibers, (**d**) mixing element, (**E**) reflectance excitation fiber, (**1**–**3**) reflectance collection locations; (right) schematic diagram of the proximal ends of the probe.

White light from a port on the side of the lamp housing is coupled to the proximal end of a single illumination fiber (80 μm, NA 0.2). Photons that scatter through the tissue and exit the surface are collected at five different positions with seven collection fibers—three located 180° from the illumination fiber (3 mm distance), two located 90° from the illumination fiber (2.1 mm), and two located 45° from the illumination fiber (1.1 mm) as shown. The proximal ends of the reflectance collection fibers are situated at the top of the vertical line of fluorescence collection fibers, separated by dummy fibers, as shown in Fig. 2.

The light source for the instrument, which provides both quasi-monochromatic excitation for fluorescence and broadband illumination for reflectance, is a 150 W ozone-free Xe arc lamp (Spectral Energy Corp., Westwood NJ) with a spherical rear reflector. A condenser system consisting of two plano-convex quartz lenses is used to couple light into a monochromator. The primary condenser is 1.5 in. in diameter with an aperture ratio of $f/1.5$. The secondary condenser is also 1.5 in. in diameter, but is masked to provide numerical aperture matching to the monochromator. A manual shutter is located between the condensing optics and monochromator and is closed to prevent fluorescence excitation light from reaching the sample during reflectance measurements. The monochromator has an aperture ratio of $f/3.6$ (Spectral Energy, GM 252) and is used with an ion-etched holographic grating (ISA, Edison, NJ; 240 nm blaze, 1180 grooves/mm, dispersion = 3.3 nm/mm). An RS-232 controlled stepper motor drives the monochromator with a maximum stepping rate of 400 step/s (approximately 10 nm/s). A bandwidth of 6.6 nm is selected by setting the entrance slit of the monochromator to 2.0 mm. Light is coupled from the monochromator into the probe via a fiber-optic adapter (Spectral Energy, GMA 257) consisting of a quartz plano-convex lens and a 5× quartz microscope objective. The light passing through the objective is focused onto a vertical line of 25 fibers in two columns, placed at the focal plane of the objective. The reflectance excitation fiber is attached to the lamp housing via a micropositioner. Broadband light exiting the lamp housing through an existing hole is coupled to the reflectance illumination fiber by using a quartz plano-convex lens (NA = 0.24). A five-position illumination filter wheel placed between the lamp and the lens contains three long-pass filters with 50% transmission at 295, 515, and 715 nm. One of the filter positions is blocked and acts as a shutter to prevent white light from reaching the sample during fluorescence measurements.

Light collected by fluorescence and reflectance fibers is coupled through an eight-position, computer-controlled collection filter wheel into a Chromex 250 IS (Albuquerque, NM) imaging spectrograph containing a holographic grating blazed at 380 nm with 150 grooves/mm and a reciprocal linear dispersion (RLD) of 20 nm/mm. The fibers are projected onto an entrance slit (250 μm) that yielded a spectral resolution of 5 nm. A thermoelectrically cooled CCD camera operated at −30 °C (Spectrasource HPC-1, Westlake Village, CA) was located at the back focal plane of the imaging spectrograph. Chip dimensions were 13.8 × 9.2 mm with 1536 × 1024 pixels (Kodak KAF-1600 grade 2), yielding a nominal spectral range of 276 nm for a single grating position. Dark current is specified as 0.25 electrons/pixel/s when operated at −30 °C. The quantum efficiency of the lumogen coated chip ranges from a peak of 40% at 550 nm to a low of 15% at 250 nm.

The detector and imaging spectrograph were wavelength calibrated by measuring the room light spectra that showed three mercury peaks at 404.7, 436, and 546 nm. The relation between pixels and wavelength was then linearly fitted through these points.

Fluorescence and reflectance measurements are obtained sequentially. Prior to fluorescence measurements, the white light port is closed and pixels illuminated by the fluorescence fibers are selected to be read from the CCD. Dark current and A/D conversion offset is measured with the same setting as the subsequent measurement but with a closed camera shutter. These are subtracted from all fluorescence and reflectance measurements. The first excitation wavelength is selected by scanning the excitation monochromator, the emission filter wheel is rotated to select the appropriate long-pass filter, and the spectrograph grating is adjusted to record signal over the desired emission wavelength range. The monochromator and camera shutters are then opened for the desired exposure time to record the fluorescence emission spectrum (1.5 s). The excitation wavelength is then incremented, and the process repeated until all desired excitation wavelengths have been measured. The excitation wavelengths were incremented from 330 to 500 nm in 10 nm steps. Table I contains a list of the

TABLE I. Fluorescence long-pass and diffuse reflectance filters used. Fluorescence long-pass filters are shown with the corresponding fluorescence excitation wavelength. Diffuse reflectance filters are shown with the corresponding measurement range.

Fluorescence long-pass filter	Fluorescence excitation wavelengths (nm)
(1) GG 375	330, 340
(2) GG 395	350, 360
(3) GG 420	370, 380, 390
(4) GG 445	400, 410, 420
(5) GG 475	430, 440
(6) OG 495	450, 460
(7) OG 515	470, 480
(8) OG 530	490, 500
Reflectance filter	**Possible reflectance measurement range**
(1) WG 295 + GG 375	350–628
(2) OG 515 + GG 375	500–778
(3) RG 715 + GG 375	700–978

excitation wavelengths and corresponding long-pass filters and emission wavelength ranges used in this study. Following collection of fluorescence spectra, diffuse reflectance spectra are then measured. For these measurements, the monochromator shutter is closed, the emission filter wheel is set to the lowest filter position, and the pixels illuminated by the corresponding reflectance collection fibers are selected to be read from the CCD. Dark current and A/D conversion offsets are measured and stored for subtraction of the following measurements. The reflectance spectrum is collected over three illumination wavelength ranges. Prior to measurement of each range, the appropriate long-pass filter is selected in the illumination filter wheel, and the spectrograph grating is adjusted to record signal over the desired wavelength range. The lamp and camera shutters are then opened for the desired exposure time to record the reflectance spectrum (0.4–4.8 s). The illumination wavelength range is then incremented, and the process repeated until all desired wavelength ranges have been measured. Exposure times are determined empirically to achieve an SNR greater than 20. Table I contains a list of the illumination wavelength ranges and corresponding long-pass filters used for diffuse reflectance measurements. The high dynamic range of the reflectance measurements, spanning over three orders of magnitude, requires that each spatial position be read out individually from the CCD. This approach prevents saturation and blooming artifacts.

There are no accepted safety standards for illumination of mucosal surfaces other than skin and cornea. However, we calculated the exposure of solar radiation that is equivalent to the exposure received when a measurement is made with our system. The method compares the spectral irradiance (W/cm^2 nm) of the excitation source with solar irradiance data obtained from Ref. 40. The comparison consists of a point-wise division of the irradiance from the FastEEM system to the solar irradiance at the same wavelength. This ratio gives a relative solar exposure factor. The solar data are for a sunny day in San Diego, CA. Irradiation during fluorescence excitation is less than 7 times solar exposure at all wavelengths. Given that fluorescence excitation times were 1.5 s, this corresponds to exposure to solar radiation for less than 11 s in any given wavelength band. During diffuse reflectance measurements, the lamp exposure is maximum at 300 nm, where the relative exposure is a factor of 25 that of the sun. Since the total exposure time for this wavelength band is 14 s, the exposure corresponds to 350 s or less than 6 min. All other wavelengths have relative exposure factors of 10 or less, resulting in a shorter equivalent total solar exposure.

Prior to every patient measurement, the probe output was measured with a calibrated power meter (Newport, Irvine, CA, 818-UV) at 400 nm excitation wavelength. An average output of 86 μW ±12 μW was achieved at this wavelength with a bandwidth of 6.6 nm. Background fluorescence spectra were measured with the probe dipped in a nonfluorescent bottle containing distilled water. This background EEM was subtracted from all subsequently acquired EEMs to correct for room lights and probe autofluorescence. The nonuniform spectral response of the system was corrected by using correction factors determined from measurements of calibration sources; in the visible, we used a National Institute of Standards and Technology (NIST) traceable tungsten ribbon filament lamp, and in the UV, we used a deuterium lamp (550C and 45D, Optronic Laboratories Inc., Orlando, FL). Variations in the intensity of the fluorescence excitation light source at different excitation wavelengths were corrected by using measurements of the intensity at each excitation wavelength at the probe tip with the use of a calibrated photodiode (818-UV, Newport). Background spectra to correct reflectance measurements for room light contributions were measured with all parameters set as for tissue measurements, except that the white light shutter was closed. These measurements were subtracted from all subsequent reflectance spectra.

Fluorescence and reflectance standards were measured before each patient measurement. The fluorescence intensity is reported relative to the fluorescence intensity of a solution of 2 mg/L Rhodamine 610 (Exciton, Dayton, OH) in ethylene glycol at 460 nm excitation and 580 nm emission. Reflectance data are reported with respect to a 2.68%-by-volume solution of 1.072 μm diameter polystyrene microspheres (Polyscience Inc., Warrington, PA). The microsphere standard was used for its well-characterized optical properties. The total integrated reflectance of this standard was measured on a double-beam spectrophotometer (U-3300 Hitachi, Tokyo, Japan) with an integrating sphere attachment (Labsphere Inc., North Sutton, NH). This measurement was used to correct the reflectance standard measurements made with the FastEEM system. Tissue spectra at each collection fiber position were divided pointwise by the corrected standard reflectance spectrum at the corresponding fiber position.

The EEMs were assembled offline from each series of fluorescence emission scans. Data processing and plotting were performed with Matlab (The Math Works Inc., Natick, MA). Reflectance spectra were assembled from three wavelength areas, giving a range from 380 to 950 nm. The wavelength range was further reduced (380–800 nm) to comply with the range of calibration measurements of the reflectance standards on the U-3300. Reflectance data are reported between 380 and 595 nm, a range where the possible influence of room lights in the measurement was minimized.

System Validation. The system performance was assessed by using two fluorescence standards. The first standard was a 2 mg/L Rhodamine 610 (Exciton Inc., Dayton, OH) ethylene glycol solution, which is nonscattering but has peak fluorescence intensity approximately twice the average intensity of human cervix.[41] The second standard mimics the optical properties of tissue and consists of 20 μM Flavin Adenine Dinucleotide (FAD, Kodak, Rochester, NY), 0.625 vol % polystyrene microspheres (Polyscience Inc., diameter = 1.072 μm).[42]

Both standards were measured with the FastEEM system and a scanning spectrofluorimeter (SPEX, Fluorolog II, Edison, NJ). The EEMs measured with the SPEX were considered as standards since the performance of the system is well documented (dynamic range = 10^5, spectral resolution 5 nm, corrected for nonuniform spectral response). The excitation light was incident perpendicular to the sampling cuvette, and the emitted light was collected at approximately a 20° angle with respect to the excitation light. A front focus arrangement with a 10 mm cuvette was used in the SPEX. Sixty minutes was required to collect a full EEM from each sample with the SPEX.

Clinical Studies. *In vivo* data were obtained from a group of patients with known or suspected premalignant or malignant lesions of the oral cavity. The studies were reviewed and approved by the Internal Review Board of the University of Texas at Austin and the Surveillance Committee at the UT M. D. Anderson Cancer Center (Houston). Informed consent was obtained from each person in the study. Before the probe was used, it was disinfected with Metricide (Metrex Research Corp.) in accordance with the standard clinical protocol. Background fluorescence EEM and reflectance spectra were measured by dipping the fiber-optic probe in a nonfluorescent bottle filled with deionized water. These EEMs and spectra correspond to the system autofluorescence and were subtracted from all subsequently acquired EEMs for that patient. Next an EEM was measured from a Rhodamine calibration standard, and a reflectance spectrum was measured from a polystyrene solution calibration standard. The probe was then guided to the tissue site to be examined and its tip positioned flush with the tissue. A fluorescence EEM and reflectance spectra were obtained from sites within a lesion and a clinically normal site. Post-spectroscopy, a 2–4 mm biopsy of the tissue was taken from normal and abnormal sites where the probe measured spectra. These specimens were evaluated by an experienced pathologist, Bonnie Kemp, M.D., with the use of light microscopy and were classified by using standard diagnostic criteria.

Data Analysis. One of the goals of instrument development is to provide information for the identification of excitation wavelengths suitable for the differentiation of tissue of differing pathological characteristics, as well as identification of the chromophores responsible for the differences. While all such information is present in the EEMs collected, it can be difficult to extract due to the dimensionality of the data set. A method was devised to separately characterize the excitation and emission characteristics of the data set. Given that the EEM has dimensions corresponding to (λ_x, λ_m), the following autocorrelation vectors are defined:

$$x_{av}(\lambda_x) = \sum_{i=1}^{N} \mathrm{EEM}(\lambda_x, \lambda_{m_i}) \cdot \mathrm{EEM}(\lambda_x, \lambda_{m_i})$$

$$m_{av}(\lambda_m) = \sum_{i=1}^{N} \mathrm{EEM}(\lambda_{x_i}, \lambda_m) \cdot \mathrm{EEM}(\lambda_{x_i}, \lambda_m)$$

where $x_{av}(\lambda_x)$ is the excitation autocorrelation vector and $m_{av}(\lambda_m)$ is the emission autocorrelation vector. Essentially, the emission autocorrelation vector is the diagonal of the product of the EEM with its transpose, and the excitation autocorrelation vector is the diagonal of the product of the transpose of the EEM with the EEM. Note that in signal processing terms, the autocorrelation vectors, x_{av} and m_{av}, are a measure of the average signal of the EEM at each excitation or emission wavelength, respectively. In this way they provide qualitative information about an EEM.

An example with simulated data is presented in Fig. 3 to illustrate how autocorrelation vectors reflect changes in fluorescence peak positions in EEMs. Two kinds of changes are simulated in the modeled data: a shift in the excitation wavelength at which a fluorescence peak appears, and a shift in the emission wavelength at which a fluorescence peak appears. The original peak in the EEM was modeled as a single Gaussian at 380 nm excitation, 550 nm emission with a full width at half-maximum (FWHM) of 35 nm in emission and excitation wavelengths. The original peak was then shifted by 30 nm in excitation, as shown by arrow 1 in Fig. 3a. The shift in emission wavelength is shown by arrow 2 in Fig. 3a, and corresponds to a 30 nm shift in the emission peak of the original data. Three sets of autocorrelation vectors were computed: one for the EEM with the original peak, one for the EEM with the excitation wavelength-shifted peak, and one for the EEM with the emission wavelength-shifted peak. The autocorrelation vectors are shown in Fig. 3b. Comparing the vectors for the original EEM (row 1 in Fig. 3b) with the vectors from the EEM with the excitation wavelength-shifted EEM (row 2 in Fig. 3b), it is seen that the excitation autocorrelation vector is sensitive to the change in excitation wavelength but not in emission wavelength. Similarly, comparing the autocorrelation vectors for the original EEM with the vectors from the EEM with the emission wavelength shift in the peak (row 3 in Fig. 3b) shows that the emission autocorrelation vector is sensitive to the changes in emission wavelength but not excitation wavelength.

It is sometimes desirable to normalize the autocorrelation vectors to facilitate comparisons between different sets of measurements. We calculated normalized autocorrelation vectors by dividing these vectors by their root mean square (rms) value, in effect forcing the area of the vector to 1 unit of signal energy. The normalized emission autocorrelation vector is well suited for the identification of differential features in EEMs, such as the shifting or broadening of fluorescence peaks.

RESULTS AND DISCUSSION

Figures 4A and 4B show fluorescence EEMs of the nonscattering Rhodamine standard and the scattering FAD phantom obtained with the FastEEM system. Intensities are reported with respect to the Rhodamine inten-

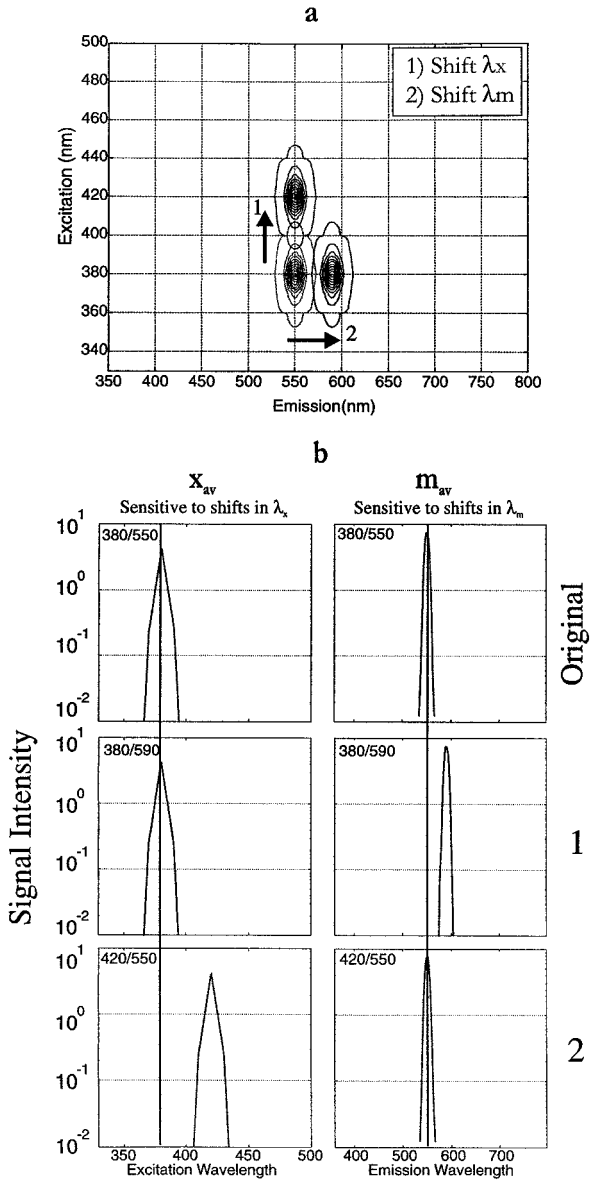

FIG. 3. (**a**) Simulated EEM with peak shifting in (***1***) excitation wavelength and (***2***) emission wavelength. (**b**) Calculated x_{av} and m_{av} for the simulated EEM. x_{av} is sensitive to changes in the excitation position of the peak, and m_{av} is sensitive to the emission position.

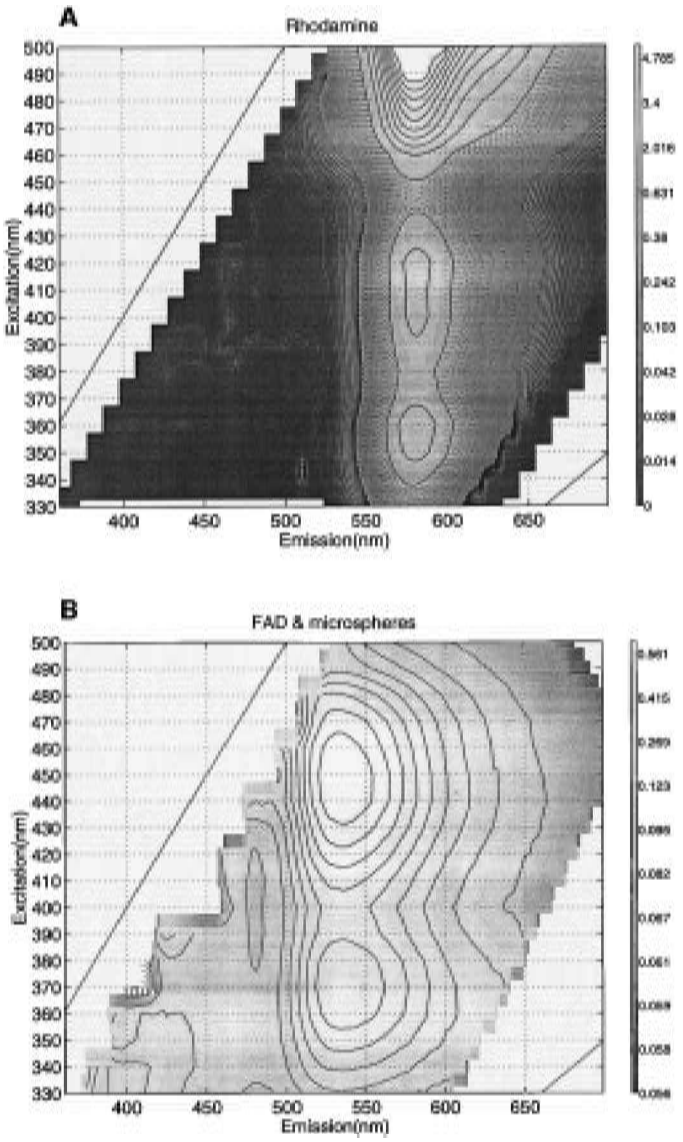

FIG. 4. (**A**) EEM of Rhodamine standard solution. (**B**) EEM of an FAD and microspheres-based tissue phantom measured with the use of the FastEEM system.

sity measured at 460 nm excitation and 580 nm emission wavelength. Figures 5a and 5c show fluorescence emission spectra of the Rhodamine standard obtained at 370 and 450 nm excitation with the SPEX and the FastEEM system as well as the fluorescence background. Figures 5b and 5d show the same spectra for scattering FAD phantom obtained at the same excitation wavelengths. The spectra are normalized at their maximum. Note the presence of Rayleigh scattering peaks from the excitation source in the data taken with the SPEX. In general, from nonscattering samples (Figs. 5a, 5c) the FastEEM system collects less light above 600 nm than the SPEX. This result could be due to the different collection efficiencies of the FastEEM probe and the front-face collection geometry of the SPEX. Under scattering conditions and with lower fluorescence signal, the influence of background fluorescence becomes more critical. At 370 nm excitation wavelength, the FastEEM system measures more fluorescence below 500 nm. A comparison with the measured fluorescence background, however, shows that the additional signal has the same shape as the background. We hypothesize that the background has been underestimated by measuring it in a nonscattering nonfluorescent media.

In vivo fluorescence EEMs of the oral cavity were measured from 71 sites, and *in vivo* reflectance spectra were measured from 49 sites. These were obtained from patients in two studies. The first study involved patients with abnormal oral lesions identified in a previous medical examination (17 patients). The second study, including nine patients, involved normal volunteers. All sites interrogated spectroscopically in patients with lesions were biopsied and submitted for histopathological analysis. Spectra and biopsies were also obtained from a contralateral site with no lesion in these patients with abnormal lesions. These biopsies were also evaluated histopathologically. No biopsies were taken from the normal

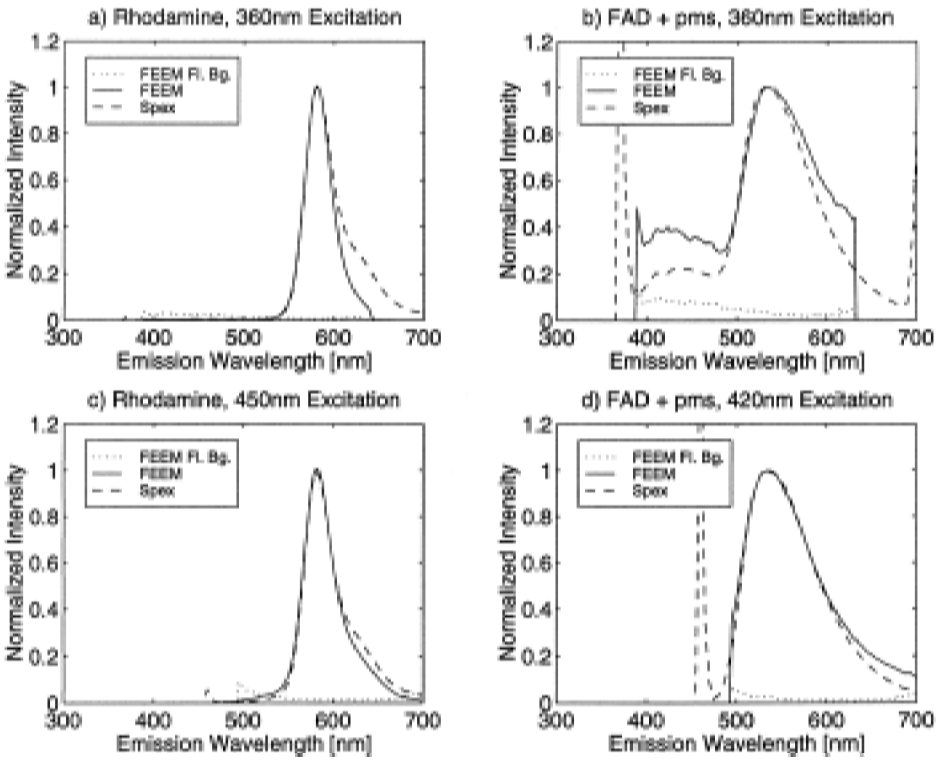

FIG. 5. (**a**) Emission spectra at 360 nm excitation of the Rhodamine calibration standard measured with the FastEEM system and SPEX Fluorolog II fluorimeter. (**b**) Emission spectra at 360 nm excitation of the scattering tissue phanthom containing FAD and polystyrene microspheres measured with the FastEEM system and SPEX Fluorolog II fluorimeter. (**c**) Emission spectra at 450 nm excitation of the Rhodamine calibration standard measured with the FastEEM system and SPEX Fluorolog II fluorimeter. (**d**) Emission spectra at 450 nm excitation of the scattering tissue phanthom containing FAD and polystyrene microspheres measured with the FastEEM system and SPEX Fluorolog II fluorimeter.

volunteers. Here, we show representative EEMs from tissue found to be histopathologically normal and malignant to illustrate spectral features detectable with the FastEEM system.

Two EEM contour plots from a normal and an abnormal area of the tongue are presented in Figs. 6A and 6B, respectively. In the normal sample, fluorescence is observed throughout the whole collection range, with a peak located at 330/380 (excitation/emission) and a ridge extending from 340/450 to 450/500 nm. Table II lists excitation-emission maxima pairs of endogenous tissue chromophores. Comparison of the observed peaks with Table II shows that these peaks are consistent with the emission of structural proteins such as collagen and elastin, pyridine nucleotides (NADH), and flavoproteins (FAD). The normal site shows overall increased fluorescence with respect to the abnormal site shown in Fig. 6B. The abnormal site, assessed by a pathologist as being moderately differentiated squamous cell carcinoma, also shows broad fluorescence throughout. Peaks are observed at 330/380, 350/460, 460/520, and 500/630 nm. A valley is seen at 420 nm excitation between 560 and 580 nm emission. This valley is seen to extend along the 420 nm excitation line as well as the 580 nm emission line. Table III suggests that these features are produced by hemoglobin reabsorption. Hemoglobin reabsorption may also in part account for the shift in the peaks of the abnormal EEM with respect to the normal EEM. A summary of the excitation and emission maxima for the peaks observed in the normal and abnormal sites measured is presented in Table IV.

Fluorescence emission spectra at three selected excitation wavelengths are shown in Fig. 7, illustrating changes in relative intensities of fluorescence emission. For comparison purposes, each set (normal/abnormal) was normalized to the maximum at 350 nm excitation. Figure 7a shows the emission spectra at 350 nm excitation. Fluorescence from the normal site is seen as a broad peak with a maximum at 455 nm. The peak from the abnormal site is seen to be narrower and red-shifted. Examination of this spectrum at 410, 540, and 580 nm suggests that the change in line shape is due to oxygenated hemoglobin. The general line shapes of the fluorescence observed at 410 nm excitation (Fig. 7b) are seen to be similar for both sites in the 450–575 nm emission range, with a broad peak at 500 nm. The abnormal site shows a significantly lower fluorescence intensity, as well as an extra, narrow fluorescence peak at 640 nm, attributed to porphyrin fluorescence. Figure 7c shows the emission spectra at 460 nm excitation. The normal site shows a broad peak at 520 nm and clear modulation from he-

TABLE II. Summary of excitation/emission maxima of endogenous tissue chromophores.

Chromophores	Excitation/emission (nm)
NADH	340/450[11]
FAD	450/515[11]
FAD	370/535[11]
Porphyrin	420/640[11]
Collagen I	340/410[43]
Collagen I	500/520[43]
Elastin	330/405[43]

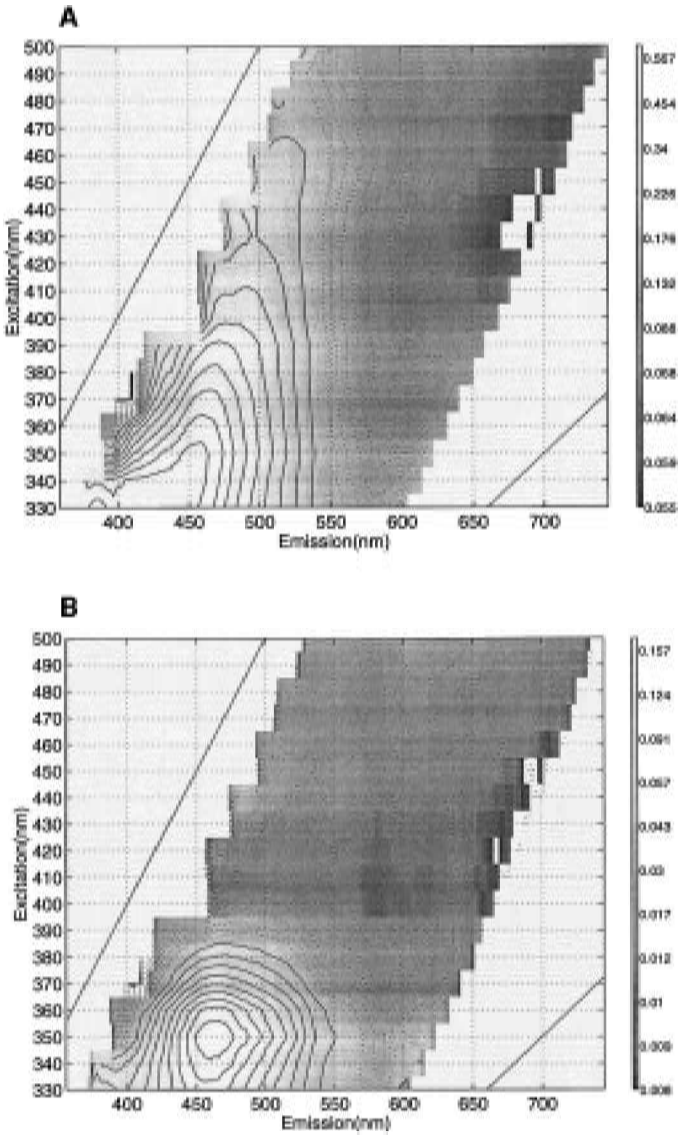

FIG. 6. *In vivo* fluorescence measurements with the FastEEM system: (**A**) Fluorescence EEM of a normal site of the tongue. (**B**) Fluorescence EEM of a diseased site of the tongue, containing a moderately differentiated squamous cell carcinoma.

moglobin reabsorption at 540 and 580 nm. Fluorescence from the abnormal site shows an even more marked hemoglobin reabsorption; also the overall fluorescence intensity is reduced.

Figure 8 shows the emission and excitation autocorrelation vectors for the same measurements. Note that the plots have a logarithmic y axis. The emission autocorrelation vectors have a large broad peak at 460 nm corresponding to the main fluorescence peak observed in the

TABLE III. Summary of absorption maxima of oxy- and deoxyhemoglobin.

Absorbers	Absorption wavelength (nm)
Oxygenated hemoglobin	415[44]
Oxygenated hemoglobin	542[44]
Oxygenated hemoglobin	577[44]
Deoxygenated hemoglobin	430[44]
Deoxygenated hemoglobin	555[44]

TABLE IV. Summary of excitation/emission maxima for peaks in the fluorescence EEMs of normal and abnormal oral cavity samples. The intensity is reported relative to the rhodamine standard at 460/580 nm.

Peak location [Excitation/emission nm]	Fluorescence intensity (Relative to rhodamine standard at 460/580 nm)
Normal site (Fig. 6A)	
330/380	0.597
340/450	0.583
450/500	0.238
Abnormal site (Fig. 6B)	
330/380	0.082
350/460	0.166
460/520	0.031
500/630	0.032

EEMs. The vectors show the effect of hemoglobin absorption around 410, 540, and 580 nm in the abnormal site and the presence of additional fluorescence in the UV in the normal sample (Fig. 8A). This autocorrelation vector also highlights the peak at 610 nm in the abnormal sample. The excitation autocorrelation vectors show different line shapes. The curve corresponding to the normal site decreases steadily from 330 to 500 nm excitation. The curve from the abnormal site shows a peak at 350 and a minimum at 410 nm. The latter illustrates the great-

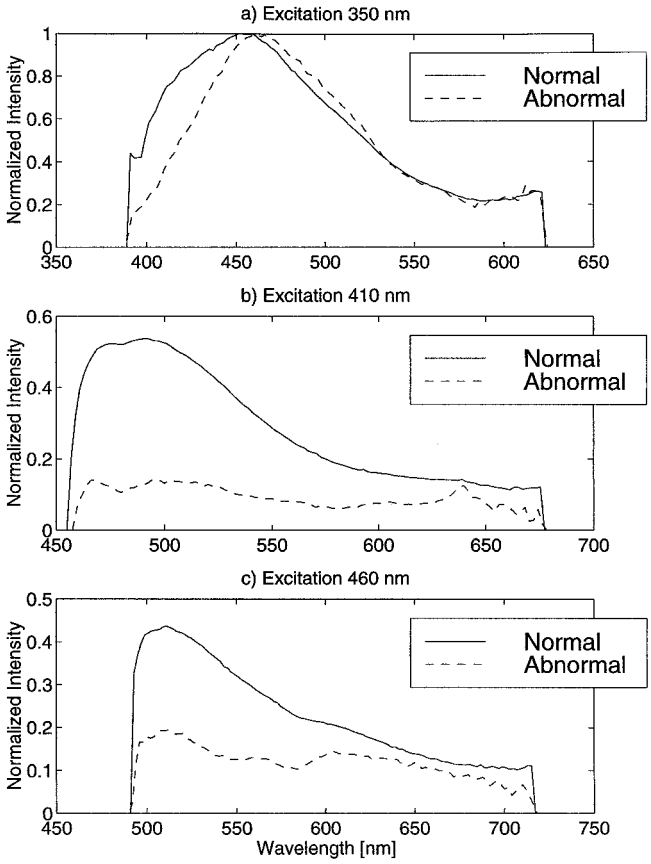

FIG. 7. Fluorescence emission spectra of normal and moderately differentiated squamous cell carcinoma of the tongue from Fig. 6. The spectra were normalized to the peak fluorescence at 350 nm excitation. (**a**) Fluorescence emission spectra at 350 nm excitation. (**b**) Fluorescence emission spectra at 410 nm excitation. (**c**) Fluorescence emission spectra at 460 nm excitation.

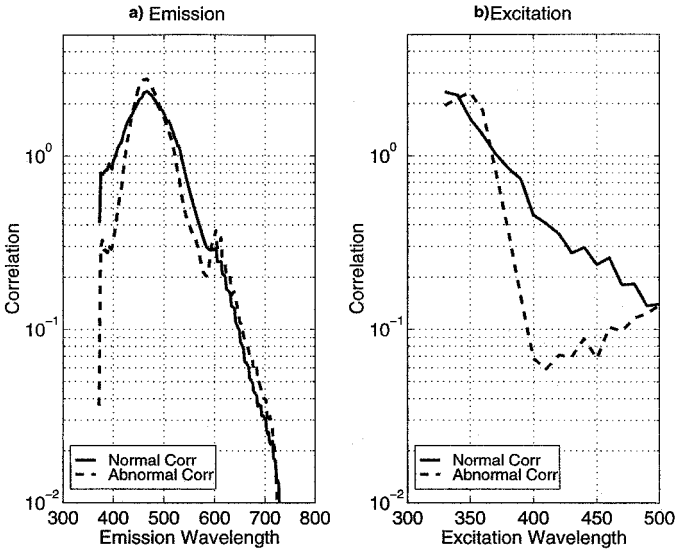

FIG. 8. Emission and excitation autocorrelation vectors of normal and moderately differentiated squamous cell carcinoma of the tongue from Fig. 6. (**a**) Emission autocorrelation vectors. (**b**) Excitation autocorrelation vectors.

er influence of hemoglobin reabsorption in the abnormal sample, also shown in Fig. 7.

The corresponding reflectance data are shown in Fig. 9. Position 1 corresponds to the collection fibers closest to the source fiber and position 3 to those furthest from the source fiber, as shown in Fig. 2. Differences induced by the fluorescence reabsorption of oxygenated hemoglobin in the normal site and abnormal site are shown. The modulation of the spectrum by the 540 and 580 nm absorption bands is seen to be significantly stronger in the abnormal sample; this observation is consistent with the increased reabsorption seen in the fluorescence spectrum of the abnormal sample. The reflectance in the blue range (450–500 nm) of the abnormal site is consistently higher than that of the normal site. Below 450 nm the reflectance seems not to differ between the normal and abnormal samples.

CONCLUSION

The total data acquisition time for the data presented here was 2.5 min for a fluorescence EEM and 1.5 min for the spatially resolved reflectance measurements. However, only 29 s of this time represents fluorescence collection. Actual reflectance collection time was 26 s. The most time-consuming process was changing the excitation wavelength by using the stepper motor-controlled excitation spectrograph and changing the corresponding long-pass filter with the use of the remotely controlled filter wheel. Worm drive-based monochromators are available (DDD180, ISA) that require less than 10 s to scan our entire wavelength range in 10 nm steps and could substantially reduce the total measurement time. Using a higher power lamp will further reduce acquisition time of both fluorescence and reflectance.

We have demonstrated the acquisition of EEMs in combination with spatially resolved reflectance measurements of tissue phantoms and in the oral cavity *in vivo* with good signal-to-noise ratio. The system features easy

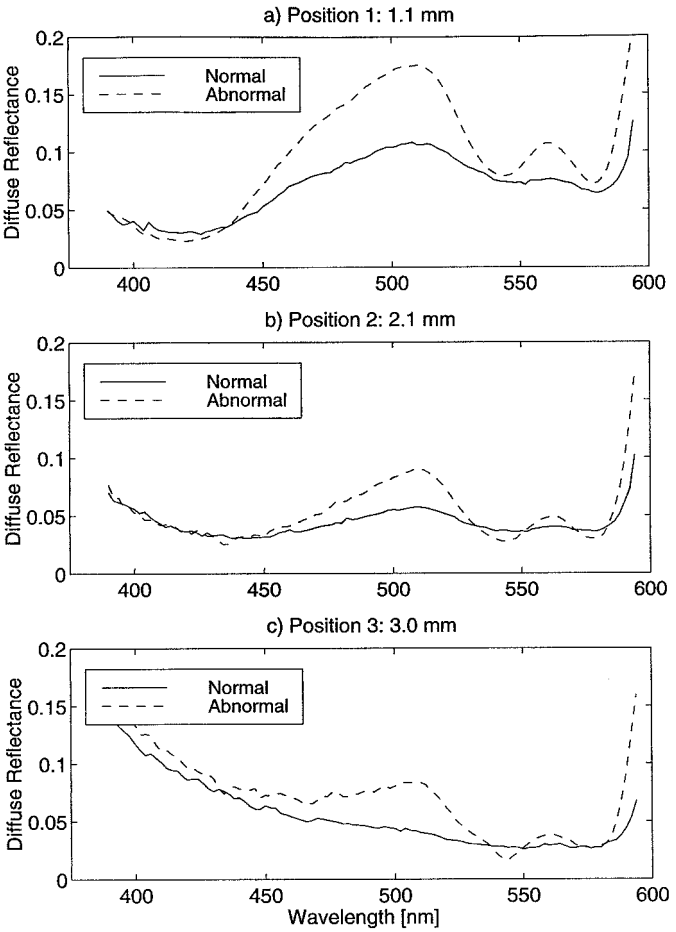

FIG. 9. Reflectance measurements of normal and moderately differentiated squamous cell carcinoma of the tongue at three different separations from the source fiber. (**a**) Position 1, 1.1 mm separation. (**b**) Position 2, 2.1 mm separation. (**c**) Position 3, 3 mm separation.

and arbitrary selection of excitation wavelengths in the UV and visible range. The system is also portable and is capable of functioning in a hospital operating room. Probes used in the FEEM system incorporate channels to measure spatially resolved reflectance and fluorescence and are made small enough (<5 mm) to be used during endoscopic surgical procedures. Autocorrelation vectors x_{av} and m_{av} are a suitable method to reduce the data set while preserving information about the wavelength bands carrying information. On the basis of the representative data shown here, fluorescence emission and excitation as well as reflectance data appear promising for the identification of tumors of the oral cavity. The FastEEM system is an ideal tool to identify a subset of the most promising optical features to identify pathological findings in large clinical studies.

ACKNOWLEDGMENT

This work was supported by a grant from the Whitaker Foundation.

1. N. J. Sterenborg, S. Thomsen, S. L. Jacques, M. Duvic, M. Motamedi, and R. F. Wagner, Jr., Dermatologic Surgery **21,** 821 (1995).
2. A. Gillenwater, paper presented at International Conference on Head and Neck Cancer, Toronto, Canada, (1996).
3. D. R. Ingrams, J. K. Dhingra, K. Roy, D. F. Perrault, Jr., I. D. Bottrill, S. Kabani, E. E. Rebeiz, M. M. Pankratov, S. M. Shapshay,

R. Manoharan, I. Itzkan, and M. S. Feld, Head & Neck **19,** 27 (1997).
4. N. Ramanujam, M. F. Mitchell, A. Mahadevan-Jansen, S. L. Thomsen, G. Staerkel, A. Malpica, T. Wright, N. Atkinson, and R. Richards-Kortum, Photochem. Photobiol. **64,** 720 (1996).
5. F. Koenig, F. J. McGovern, A. F. Althausen, T. F. Deutsch, and K. T. Schomacker, J. Urol. **156,** 1597 (1996).
6. K. T. Schomacker, J. K. Frisoli, C. C. Compton, T. J. Flotte, J. M. Richter, T. F. Deutsch, and N. S. Nishioka, Gastroenterology **102,** 1155 (1992).
7. R. M. Cothren, R. Richards-Kortum, M. V. Sivak, M. Fitzmaurice, R. P. Rava, G. A. Boyce, M. Doxtader, R. Blackman, T. B. Ivanc, G. B. Hayes, M. S. Feld, and R. E. Petras, Gastrointestinal Endosc. **36,** 105 (1990).
8. Y. Yang, A. Katz, E. J. Celmer, M. Zurawska-Szczepaniak, and R. R. Alfano, Lasers Life Sci. **7,** 115 (1996).
9. Y. G. Chung, J. A. Schwartz, C. M. Gardner, R. E. Sawaya, and S. L. Jacques, J. Korean Med. Sci. **12,** 135 (1997).
10. N. S. Nishioka, Gastrointestinal Endosc. Clinics North Am. **4,** 313 (1994).
11. R. Richards-Kortum and E. Sevick-Muraca, Annu. Rev. Phys. Chem. **47,** 555 (1996).
12. A. G. Bohorfoush, Endoscopy **28,** 372 (1996).
13. J. J. Bigio and J. R. Mourant, Physics Med. Biol. **42,** 803 (1997).
14. J. F. Holland, R. E. Teets, and A. Timmick, Anal. Chem. **45,** 145 (1973).
15. I. M. Warner, J. B. Callis, E. R. Davidsion, M. Gouterman, and G. D. Christian, Anal. Lett. **8,** 665 (1975).
16. I. M. Warner, G. D. Christian, E. R. Davidson, and J. B. Callis, Anal. Chem. **49,** 564 (1977).
17. I. M. Warner, E. R. Davidson, and G. D. Christian, Anal. Chem. **49,** 2155 (1977).
18. C.-N. Ho, G. D. Christian, and E. R. Davidson, Anal. Chem. **50,** 1108 (1978).
19. B. E. Wilson, W. Lindberg, and B. Kowalski, J. Am. Chem. Soc. **111,** 3797 (1989).
20. A. J. Durkin, S. Jaikumar, N. Ramanujam, and R. Richards-Kortum, Appl. Opt. **33,** 414 (1994).
21. A. J. Durkin and R. Richards-Kortum, Lasers Surgery Med. **19,** 75 (1996).
22. L. I. Deckelbaum, M. L. Stetz, K. M. O'Brien, F. W. Cutruzzola, A. F. Gmitro, L. I. Laifer, and G. R. Gindi, Lasers Surgery Med. **9,** 204 (1989).
23. A. Mahadevan, M. F. Mitchell, E. Silva, S. Thomsen, and R. Richards-Kortum, Lasers Surgery Med. **13,** 647 (1993).
24. R. Richards-Kortum, R. P. Rava, R. E. Petras, M. Fitzmaurice, M. Sivak, and M. S. Feld, Photochem. Photobiol. **53,** 777 (1991).
25. R. Cothren, T. Kolubayev, B. T. Kjellstrom, R. Richards-Kortum, B. Healy, N. Ratliff, G. Engelmann, F. Loop, J. R. Kramer, C. Kittrell, and M. S. Feld, Proc. SPIE–Int. Soc. Opt. Eng. **906,** 320 (1988).
26. K. T. Schomacker, J. K. Frisoli, C. C. Compton, T. J. Flotte, J. M. Richter, N. S. Nishioka, and T. F. Deutsch, Lasers Surgery Med. **12,** 63 (1992).
27. A. J. Welch, C. Gardner, R. Richards-Kortum, G. Criswell, E. Chan, J. Pfefer, and S. Warren, Lasers Surgery Med. **21,** 166 (1997).
28. R. Richards-Kortum, in *Optical-Thermal Response of Laser Irradiated Tissue,* A. J. Welch and M. Van Gemert, Eds. (Plenum Press, New York, 1994), Chap. 21.
29. T. J. Farell, M. S. Patterson, and B. C. Wilson, Med. Phys. **19,** 879 (1992).
30. L. Wang and S. L. Jacques, Med. Phys. **21,** 1081 (1994).
31. L. Wang and S. L. Jacques, Appl. Opt. **34,** 2362 (1995).
32. S. P. Lin, L. Wang, S. L. Jacques, and F. K. Tittel, Appl. Opt. **36,** 136 (1997).
33. M. G. Nichols, E. L. Hull, and T. Foster, Appl. Opt. **36,** 93 (1997).
34. J. R. Mourant, J. J. Bigio, J. Boyer, R. L. Conn, T. Johnson, and T. Shimada, Lasers Surgery Med. **17,** 350 (1995).
35. C. J. Lynn, D. G. Oelberg, and S. L. Jacques, Biol. Neonate **64,** 69 (1993).
36. A. J. Durkin, Dissertation, University of Texas at Austin, Austin (1995).
37. J. Wu, M. S. Feld, and R. P. Rava, Appl. Opt. **32,** 3585 (1993).
38. R. A. Zangaro, L. Silveira Jr., R. Manoharan, G. Zonios, I. Itzkan, R. R. Dasari, J. Van Dam, and M. S. Feld, Appl. Opt. **35,** 5211 (1997).
39. J. A. Zuclich, T. Shimada, T. R. Loree, I. Biggio, K. Strobl, and S. Nie, Lasers Life Sci. **6,** 39 (1994).
40. NSF Polar Programs UV Spectroradiometer Network 1994–1995 Operations Report; NSF UV Radiation Monitoring Network 1994 to 1995, Volume 5.0 Data Set. Available at www.biospherical.com.
41. E. V. Trujillio, D. R. Sandison, U. Utzinger, N. Ramanujam, M. F. Follen-Mitchell, and R. Richards-Kortum, Appl. Spectrosc. **52,** 943 (1998).
42. A. J. Durkin, S. Jaiumar, and R. Richards-Kortum, Appl. Spectrosc. **47,** 2114 (1993).
43. S.-H. Cheng, Master's Report, The University of Texas at Austin, Austin (1992).
44. *An Introduction to Spectroscopy for Biochemists.* S. B. Brown, Ed. (Academic Press, London/New York, 1980).